Broadening factors of E_1(LO) phonon-plasmon coupled modes of hexagonal InN investigated by infrared reflectance measurements

Yoshihiro Ishitani,* Takashi Ohira, Xinqiang Wang, Son-Bek Che, and Akihiko Yoshikawa
Graduate School of Electrical and Electronics Engineering, Venture Business Laboratory, InN project as a CREST program, JST, Chiba University, 1-33 Yayoicho, Inage-ku, Chiba 263-8522, Japan
(Received 24 October 2006; revised manuscript received 5 February 2007; published 10 July 2007)

The LO phonon-plasmon coupling of InN for the E_1(LO) mode has been found; however, the decoupling for the A_1(LO) mode has been reported in many issues. Several reports have discussed the electron- and phonon-scattering mechanisms, while there is no detailed investigation on the broadening factors of mode energies even for E_1(LO) phonon-plasmon coupled scheme. In this issue, the studied InN layers grown by the molecular-beam epitaxy method have residual electron density obtained by Hall measurements in a range from 8×10^{17} to 1×10^{19} cm^{-3}. The electron density measured by infrared reflectance measurements is almost constant with a temperature variation from 5 to 300 K. The dependence of the observed broadening factors of the E_1(LO) phonon-plasmon coupled modes on the electron density is found to show the characteristic properties of the level anticrossing, in particular, for the increase of these broadening factors around the level anticrossing region with the temperature increase from 5 to 300 K. Compared to the recent report on the LO phonon-plasmon coupled modes for A_1(LO), smaller broadening for E_1(LO) is observed here.

DOI: 10.1103/PhysRevB.76.045206 PACS number(s): 63.20.Kr, 78.30.Fs

I. INTRODUCTION

The progress in the InN growth by the molecular-beam epitaxy (MBE) method led to the decrease in the residual electron density (n_e) to the order of 10^{17} cm^{-3}. Recent researches report the band-gap energy values (E_g's) of 0.63–0.8 eV (Refs. 1–3) and 1.4 eV (Ref. 4) and the effective electron mass values (m_e's) of $0.04m_0$–$0.14m_0$.[5–8] We found that E_g of about 0.67 eV and m_e of $0.046m_0$ around 10 K are in good agreement with the photoluminescence and absorption spectra, and obtained the experimental transition matrix element of about $1.0\hbar^2/2m_0$ Ry.[9] In most of the reports, n_e/m_e was obtained from the energy of the higher-energy branch of the E_1(LO) phonon-plasmon coupled (LOPC) modes by the analysis of infrared (IR) reflectance or spectroscopic ellipsometry with assumptions of the complete LOPC for the E_1(LO) mode and the agreement of n_e from the optical spectra with Hall electron density (n_H). Since the nonparabolic conduction band edge structure has been reported, the LOPC analysis based on the dispersion of m_e is now required.

The LO phonon-plasmon coupling in degenerate polar semiconductors has been investigated in detail.[10–12] Giehler and Jahne reported a strong LOPC feature in the mode broadening factor for CdS.[11] Singwi and Tosi theoretically stated that the overdamping leads to the crossing of the two modes in general: disappearance of the anticrossing of the LOPC states.[12] Experimental overdamping features are observed for several materials.[11,13] However, there are few reports on the dependence of the broadening factors on temperature. At present, most of the InN layers have the threading dislocation density more than 10^{10} cm^{-2} or more.[14,15] There are studies reporting the electron scattering at dislocations of InN as a main factor on electron mobility from its dependence on temperature.[16,17] The energetic properties of InN phonon modes are studied in detail;[18] however, there are few detailed reports on the effect of the phonon or electron scattering at crystal defects on the broadening factors of plasmon and LOPC modes. There is a controversial matter of the LO phonon-plasmon coupling condition of InN. Although Kasic *et al.* and Darakchieva *et al.* reported the coupling of the A_1(LO) mode with plasmon by spectroscopic ellipsometry measurements,[5,19] the decoupling for the A_1 mode was reported by Raman measurements.[17,20–23] Inushima *et al.* reported no coupling of the A_1(LO) mode for an n_H range of 1.8×10^{18}–1.5×10^{19} cm^{-3} by Raman spectra.[20] As for the origin of this decoupling, there are several discussions: the Fano interference effect of the quasicontinuum electronic state and the zone-center LO phonon[20] and the scattering with large wave-vector transfer by charge-density fluctuation.[22] In the measurements of the ellipsometry on InN, the broadening factors of LOPC modes were assumed to be isotropic.[5] Further, A_1(TO) mode energy obtained from Raman measurements was utilized.[5,18] Therefore, the difference in the coupling behaviors between the E_1(LO) and A_1(LO) modes was not investigated in view of the broadening factors. Although the energetic LOPC behavior was found for E_1(LO) phonon-plasmon system in many reports, the dependence of the broadening factors of the LOPC modes on n_e has not been investigated even for this mode. As for the dependence of the phonon properties on temperature, Pomeroy *et al.* reported that phonon lifetime of InN decreases from 0.4 to 0.6 ps with the increase in the temperature range from 80 to 300 K.[24] However, the dependence of the broadening factors for the LOPC modes has not been investigated. As a fundamental knowledge for the scattering condition of the LO phonon-plasmon system for InN layers of present status, we investigate the dependence of the broadening factors of the E_1(LO) phonon-plasmon coupled states on the electron density and crystal temperature by *s*-polarized IR reflectance measurements, and discuss the scattering of LOPC states.

II. EXPERIMENTAL AND SPECTRUM ANALYSIS METHOD

Crystal growth was performed by plasma assisted MBE method. InN epitaxial layers were grown at 500–630 °C on InN buffer layers grown around 450 °C or GaN epitaxial layers[14] on α-Al_2O_3 (sapphire) (0001) substrates. We found the dislocation density of the order of 10^9 or 10^{10} cm^{-2}.[14,15] A few samples with n_H in the order of 10^{17} cm^{-3} had the $+c$ surface polarity. The other samples had the $-c$ polarity. The thickness of the typical samples was about 2 μm or larger, which was measured by a scanning electron microscope or a confocal optical microscope. Hall measurements were performed at room temperature (RT); n_H was in a range of $8.3\times10^{17}-1.8\times10^{19}$ cm^{-3}. Most of the samples had larger Hall mobility than 1000 cm^2/V s. X-ray rocking curves were obtained for (0002) and $(10\bar{1}2)$ diffractions at RT.

IR reflectance measurements were carried out using a Fourier transform IR (FTIR) measurement system and a cryostat. The incidence angle of the IR light was 30° inclined from the surface normal. The *s* polarization of the incident light was selected by a polarizer made of KRS-5. The resolution of the system was 2 cm^{-1}. During the measurements, nitrogen gas was flowed along the optical path of the FTIR system. The reflectivity was calculated using the reflectance spectrum of a gold film on a glass plate. The sample temperature was controlled at 5 or 300 K.

The reflectance spectra of multilayer structures were calculated by the transfer-matrix method. We analyzed the dielectric function for the component normal to the *c* axis. For α-Al_2O_3, the phonon energies and their broadening factors obtained from the least-squares fit of the experimental spectrum were almost the same with the former reports: within 3 cm^{-1} for phonon energies.[25,26] As the dielectric constants of $\varepsilon(\infty)$ and $\varepsilon(0)$, $3.06\varepsilon_0$ and $9.33\varepsilon_0$ were adopted, respectively.[25,26] Here, ε_0 stands for the value in the vacuum.

The dielectric functions of InN and GaN layers were analyzed with the use of the following widely used formula, in which the energies of the E_1(LO) phonon-plasmon coupling were explicitly expressed:[5,26]

$$\varepsilon(E)=\varepsilon(\infty)\frac{(E^2-E_+^2+i\gamma_+E)(E^2-E_-^2+i\gamma_-E)}{(E^2+i\gamma_pE)(E^2-E_{\mathrm{TO}}^2+i\gamma_{\mathrm{TO}}E)}. \quad (1)$$

Here, E_+ and E_- represent the energies of LOPC+ and LOPC− modes, respectively. These $E_\pm$ are expressed as $\{[E_e^2+E_{\mathrm{LO}}^2\pm\sqrt{(E_e^2+E_{\mathrm{LO}}^2)^2-4E_e^2E_{\mathrm{TO}}^2}]/2\}^{1/2}$. E_e is the plasma oscillation energy of $\hbar\sqrt{n_e e^2/\varepsilon(\infty)m_e}$. The broadening factors for TO phonon energy (E_{TO}), plasmon energy, E_+, and E_- are denoted by γ_j (j=TO, p, +, and −). For GaN, $\varepsilon(\infty)$ of $5.04\varepsilon_0$ was taken from Ref. 26. For InN, it was obtained by the spectrum fitting for the oscillation structure with the use of the film thicknesses of InN and GaN. Some of the parameters for GaN were obtained using a single GaN layer on the substrate, where E_{TO} of 560 cm^{-1}, γ_p, γ_+, and γ_- of 140, 7, and 135 cm^{-1}, respectively, and n_e of 1×10^{17} cm^{-3} were obtained using m_e/m_0 (m_e^*) of 0.2. The ratio of E_{TO} and the LO phonon energy was taken from Refs. 5, 7, and 26. These values were utilized in the following analysis.

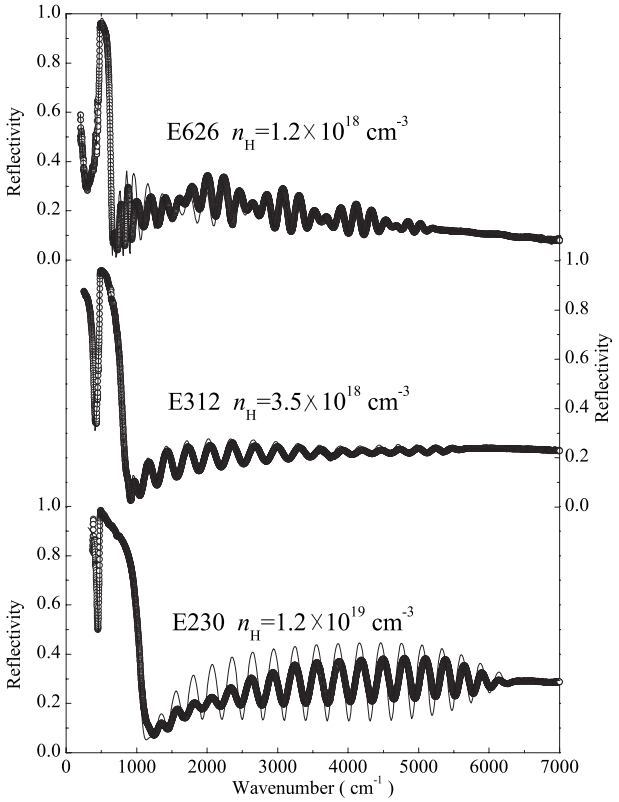

FIG. 1. IR reflectance spectra at 300 K in an energy range from the LOPC region to the electronic band edge energy region. The solid curves are the best-fit functions by the formula of the sum of Eq. (1) and the dielectric function for the electronic band-band transition represented in the former issue (Ref. 9).

The effective mass of InN was calculated with the use of the dependence of the conduction-band (CB) electron energy (E_c) on electron wave vector (k_e),[6,27]

$$E_c(k_e)=E_g+\frac{\hbar^2k_e^2}{2m_0}+\frac{1}{2}\left(\sqrt{E_g^2+4E_p\frac{\hbar^2k_e^2}{2m_0}}-E_g\right). \quad (2)$$

The formula $m_e=\hbar^2k_e/(dE_c/dk_e)$ was also utilized. The wave vector at the Fermi surface is expressed by $k_{e,F}=(3\pi^2n_e)^{1/3}$. Here, the band-gap energy E_g was taken as 0.675 eV at cryogenic temperature. The parameter E_p was taken as 14 eV, which gives the transition-matrix element of $1.0\hbar^2/2m_0$ Ry and m_e^* of 0.046 at the conduction-band bottom.[9]

III. RESULTS

A. Overall reflectance spectrum characteristics of InN layers

Figure 1 shows the reflectance spectra at 300 K for the samples with the thickness of about 5 μm or larger. The increase in the fundamental absorption edge with the increase in n_H is shown. From the analysis of the absorption and photoluminescence spectra for samples with the thickness of about 1 μm and n_H of about $(0.8-1)\times10^{18}$ cm^{-3}, we have obtained the consistent fitting of the photoluminescence and absorption spectra by taking account of the Burstein-Moss effect and the nonparabolic CB energy structure ex-

TABLE I. Characteristic properties of InN layers. The values except for γ_p and n_e/m_e^* are at 300 K or RT. The data of γ_p and n_e/m_e^* are obtained from the spectra at 5 K. Equation (2) is used for the calculation of n_e. E695 has the $+c$ surface polarity.

Sample ID	E695	E626	E472	E312	E230
n_e/m_e^* (10^{19} cm^{-3})	0.60	0.97	2.6	3.7	10.0
n_e (10^{18} cm^{-3})	0.30	0.50	1.5	2.2	7.4
γ_p (cm^{-1})	80	98	123	62	162
$\varepsilon(\infty)/\varepsilon_0$	7.0	7.0	7.1	7.4	9.0
Hall mobility (cm^2/V s)	2030	1300	1150	1200	730
FWHM of XRD rocking curve for (0002) (arc sec)	380	530	370	450	1400
FWHM of XRD rocking curve for $(10\bar{1}2)$ (arc sec)	1100	1330	1450	670	2200

pressed in Eq. (2).[9] With the same model function, we fitted the reflectance spectra. The solid curves in Fig. 1 are the best-fit functions for the respective spectra. They agree well with the experimental results. This result indicates that the present CB edge energy structure is applicable to the investigation for LOPC properties.

From the interference oscillation structure of the reflectance spectra, we obtained $\varepsilon(\infty)$ for each sample. For E626 with n_e of $1\times10^{19}m_e^*$ cm^{-3}, we obtained 7.0 $(\pm0.3)\varepsilon_0$, which agrees with the former result of $6.7\varepsilon_0$.[18] The values for typical examples are listed in Table I. This constant increases with the increase in the residual electron density. It is estimated that the crystal defects generating electrons in the CB bottom are a candidate origin of the increase in $\varepsilon(\infty)$. The decrease in $\varepsilon(\infty)/\varepsilon_0$ from 9.0 to 7.0 for the fitting of the spectrum of E230 causes the decrease in n_e/m_e^* by 20% and almost no change in the broadening factors. For samples with smaller n_e/m_e^* than 5×10^{19} cm^{-3}, this effect of the variation in $\varepsilon(\infty)$ on the parameters is smaller.

Figure 2 shows magnified spectra in a region from

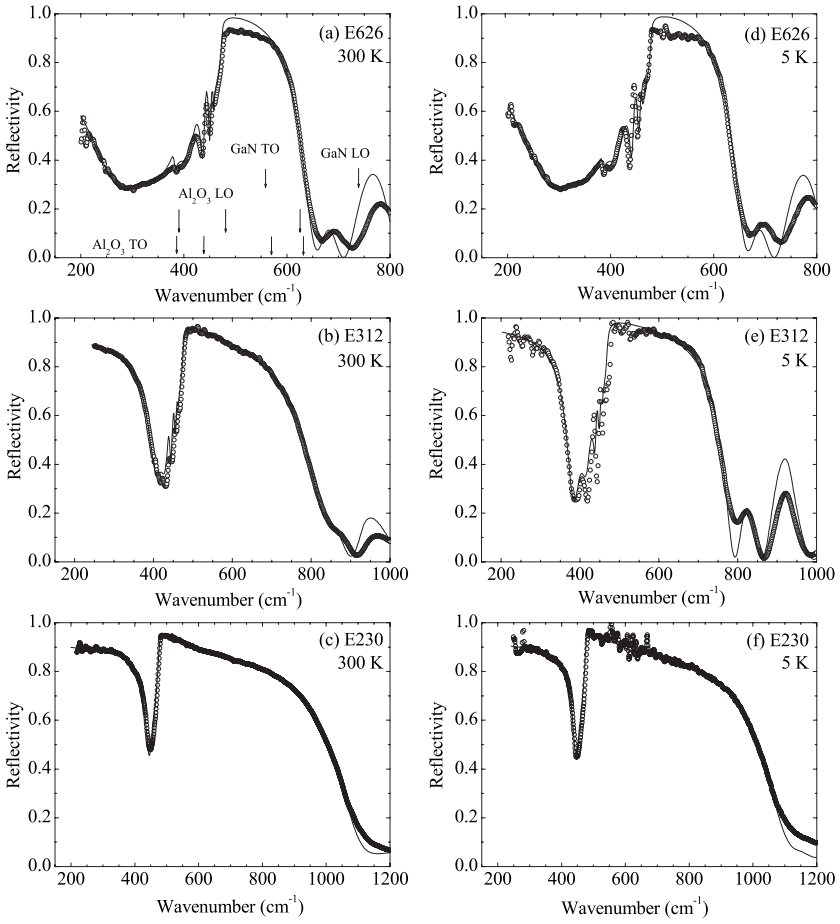

FIG. 2. IR reflectance spectra in the LOPC energy region: (a), (b), and (c) at 300 K, (d), (e), and (f) at 5 K, (a) and (d) for E626, (b) and (e) for E312, and (c) and (f) for E230. The arrows in (a) indicate the energy positions of the TO and LO phonons of α-Al_2O_3 substrates and GaN. Open circles are the experimental plots. The solid curves are the best-fit functions.

200 to 1000 cm^{-1}. Figures 2(a)–2(c) are the spectra at 300 K. The TO and LO phonon energy positions for α-Al_2O_3 and GaN are indicated by arrows in Fig. 2(a). These figures show that the eminent structures of the spectrum edge positions are not for the phonon modes of α-Al_2O_3 substrate or those of GaN layers. The edge position around 475 cm^{-1} agrees with the E_1(TO) phonon energy of InN. We conducted least-squares fits of the experimental spectra in both the energy regions for LOPC− and LOPC+ modes. Here, in addition to the E_1(TO) phonon energy, n_e/m_e^*, γ_+, γ_-, and γ_p of InN were adjusted.

For samples with smaller n_e/m_e^* than 1×10^{19} cm^{-3}, we took account of nonuniform electron distribution in InN layers: electron accumulation (EA) regions just above the InN/GaN interface and around columnar crystal domains along the c axis. Electrons were supposed to be accumulated in the dip of the bended CB bottom within the thickness of tens of nanometers around the surface and interface.[28,29] This bending is generated by the levels of high-density crystal defects including dislocations around the interface and columnar grain boundaries. These models are in accordance with the observation of high-density dislocations of the order of 10^9 or 10^{10} cm^{-2} and the columnar structures observed by tunneling electron microscopy or atomic force microscopy.[13,14] We found that the effect of the surface accumulation was minor to above two factors. This may be caused by the large broadening of the plasmon around the surface. The detail will be discussed elsewhere. The account of these EA structures brings us the decrease of n_e in the order of $10^{18}m_e^*$ cm^{-3} for the bulk region except for the EA regions. This factor does not affect the interpretation of the final result shown later for the dependence of the broadening factors on n_e/m_e^*. For samples with larger n_e/m_e^* than 1×10^{19} cm^{-3}, the model of a single InN layer with a uniform electron distribution fits the spectra. This result is ascribed to the large sheet electron density of the order of $10^{15}m_e^*$ cm^{-2} compared to those of EA structures of $10^{14}m_e^*$ cm^{-2}. The solid curves in Fig. 2 are the best-fit functions at 5 and 300 K. The small deviation at the Reststrahlen band for Figs. 1(a) and 1(d) was ascribed to the rough surface from the analogy of the GaAs case reported by Holm and Palik.[30]

B. Dependence of the broadening factors of LOPC modes on electron density

The dependence of γ_+ and γ_- on n_e/m_e^* at 5 K is depicted in Fig. 3(a). The increase in γ_+ and the decrease in γ_- with the increase in n_e are shown in this figure. This feature is interpreted in the scheme of LOPC as follows. Figure 4 shows the calculated dependence of E_+, E_-, and E_e on n_e/m_e^* under a condition of E_p=14 eV and E_g=0.675 eV. Here, n_e/m_e^* is taken as the abscissa in accordance with the quantity directly obtained by the IR reflectance spectra. The obtained adjusted parameters of n_e/m_e^* and γ_p at 5 K are listed together with the other properties measured at RT in Table I. Figure 4 indicates that for InN, the plasmonlike property of the LOPC− mode appears below n_e of $(3-4.5)\times10^{19}m_e^*$ cm^{-3} where the energy level anticrossing takes place. For the region of larger n_e than this value, it is thought

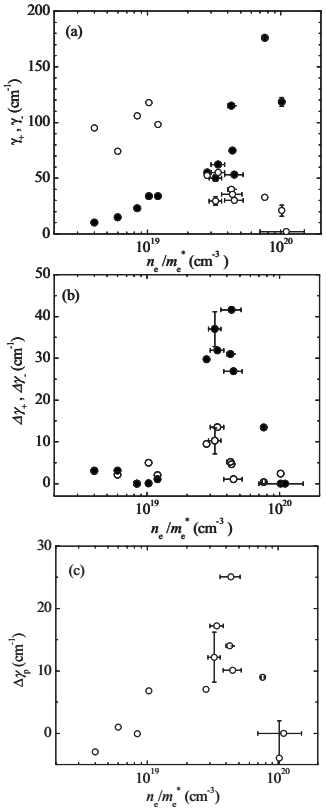

FIG. 3. Dependence of the broadening factors on electron density: (a) γ_+ (●) and γ_- (○) at 5 K, (b) $\Delta\gamma_+$ (●) and $\Delta\gamma_-$ (○), and (c) $\Delta\gamma_p$. The electron densities are taken as the average values of those at 300 and 5 K. The typical error ranges for ordinate quantity are drawn for some typical samples.

that the LOPC− mode shows the screened or bare LO phonon (B-LO) property.[30,31] On the other hand, for higher-energy mode, this n_e value of $(3-4.5)\times10^{19}m_e^*$ cm^{-3} is the boundary between the LO phonon behavior and the plasmon one. As the experimental result, we obtained γ_p of around 80 cm^{-1} or larger and γ_{TO} of 3–5 cm^{-1}. This result is interpreted as follows. As the character of the LOPC+ mode transfers from the LO phononlike character to the plasmonlike one,[10] γ_+ increases with the increase in n_e. For the

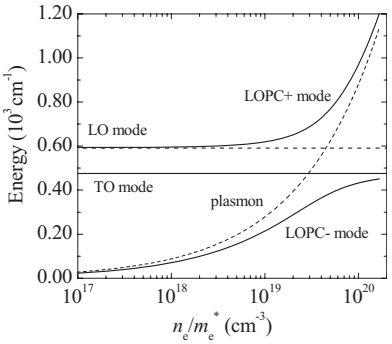

FIG. 4. Calculated anticrossing behavior of plasmon and E_1(LO) phonon energies. E_p of 14 eV and E_g of 0.675 eV are adopted in the calculation. Two solid curves and a line correspond to the IR active modes for the present experimental geometry.

LOPC− mode, γ_- decreases in accordance with the transfer from the plasmonlike property to the B-LO one. Therefore, it is thought that the two broadening factors of the respective two modes in reflectance spectra of InN are interpreted to obey the LO phonon-plasmon coupling or the screening of the macroscopic electric field of the LO phonon by electrons.

C. Effect of temperature increase on the broadening factors

We compare the effect of the temperature increase from 5 to 300 K on the spectrum between samples E626, E312, and E230 K. For E626 and E230, the spectra of these two temperatures are almost identical, while the spectrum of E312 varies with temperature, in particular, for an energy range of 600–900 cm^{-1}. For E312, with the temperature increase we detected an increase in γ_+ from 50 to 86 cm^{-1} and a slight increase in n_e/m_e^* from 2.9×10^{19} to 3.7×10^{19} cm^{-3}. The increases in γ_+ and γ_- with the increase in temperature from 5 to 300 K are denoted by $\Delta\gamma_+$ and $\Delta\gamma_-$, respectively. Figure 3(b) shows that the dependence of $\Delta\gamma_+$ and $\Delta\gamma_-$ on n_e/m_e^*. For samples showing the increase in n_e/m_e^* with the temperature increase, the average values for 5 and 300 K are taken for the abscissa; the error bars indicate the variation of n_e/m_e^* with the temperature increase. The peak positions of $\Delta\gamma_+$ and $\Delta\gamma_-$ are located around n_e/m_e^* of $3–4.5\times10^{19}$ cm^{-3}. This value corresponds to $n_e=(1.5–2.3)\times10^{18}$ cm^{-3} from Eq. (2). The variation of E_p of 10–14 eV (Refs. 1 and 3) leads to the variation of n_e by 40%. This n_e/m_e^* agrees with the theoretical anticrossing region of $(3–4.5)\times10^{19}$ cm^{-3} shown in Fig. 4. The increase in n_e/m_e^* for E312 with the temperature increase contributes to an increase in γ_+ by about 10 cm^{-1} at most, which was estimated from the dependence of γ_+ on n_e of Fig. 3(a). Sample E472 has $\Delta\gamma_+$ of 29 cm^{-1}, while it has no variation of n_e with the temperature increase. Thus, the increase in n_e does not explain the increase in $\Delta\gamma_j$'s.

With account of the dependence of γ_+ and γ_- on n_e/m_e^*, we ascribed this enhancement of $\Delta\gamma_j$'s in the anticrossing region to an enhancement of the scattering rate of LOPC states: depopulation of LOPC states, the excitation and deexcitation transfer between LOPC+ and LOPC− states, and so forth. As shown in Fig. 3(c), $\Delta\gamma_p$ is also enhanced around the anticrossing region to a value of 25 cm^{-1}. This result indicates that LOPC characterizes the scattering of electrons. Thus, the enhancement of $\Delta\gamma_p$, $\Delta\gamma_+$, and $\Delta\gamma_-$ at n_e/m_e^* of $(3–4.5)\times10^{19}$ cm^{-3} reveals the strong electron-phonon coupling around the energy anticrossing point.

IV. DISCUSSION

As shown in Fig. 3(b), the peak value of $\Delta\gamma_+$ around the anticrossing region is larger than that of $\Delta\gamma_-$. There are two possible explanations. The first candidate explanation is based on the fact that γ_p increases with the increase in temperature in the anticrossing region, and this increase is larger than that for phonons, which was shown by Pomeroy *et al.* for InN with the use of Raman spectra: the increase from 4 cm^{-1} at 80 K to about 8 cm^{-1} at RT for the uncoupled A_1(LO) phonon.[23] The γ_- value of 20 cm^{-1} for E230 indicates that the B-LO phonon has the small broadening factor. The small increase in γ_- for samples with high n_e/m_e^* such as E230 agrees with the fact that the broadening factors of the LO phonon and TO phonon have smaller dependence on temperature. Since the lower-energy branch transfers from the plasmonlike mode to the B-LO phonon mode with the increase in n_e, the smaller $\Delta\gamma_-$ than $\Delta\gamma_+$ and $\Delta\gamma_p$ indicates that the LOPC− mode around the anticrossing region is nearly dominated by the B-LO phonon mode: the dependence of the broadening factor of the LOPC+ mode shows plasmonlike property as a main factor in the anticrossing region. The increase in the broadening factors with temperature was attributed to the Fröhlich interaction, anharmonic lattice vibration, the scattering at crystal defects, and so forth. However, there is an unclear point: why the B-LO phonon mode is dominant at the anticrossing point, where LOPC modes are not pure plasmon or phononlike mode energetically. The peak of $\Delta\gamma_p$ around the anticrossing point is thought to be caused by the high scattering rate of plasmons by the strong LO phonon-plasmon coupling. The second possible reason for the smaller $\Delta\gamma_-$ is the smaller rates of depopulation and excitation transfer for the LOPC− mode than those of the depopulation and deexcitation transfer for the LOPC+ mode. Since all of the LOPC+, plasmon, and phonon states are located at higher energy levels than the LOPC− mode, these energy differences would lead to threshold energies for the cross sections of the depopulation and excitation transfer processes. These increases in the scattering rate with the increase in temperature would be caused by the excitation of the lattice vibration modes or increase in the phonon occupation factor, leading to the increase in the Fröhlich interaction, the anharmonic lattice vibration, the thermal excitation of electron kinetic energy, and so forth. The excitation and deexcitation processes between LOPC states are also possible because such transfer processes around the level anticrossing point have been observed for various physical systems: Landau-Zener transition between molecular states, collisional excitation and deexcitation transfer of atomic states in magnetic field, and so forth.

Giehler and Jahne obtained a result of mode broadening factors for CdS at 300 K.[11] They showed the enhancement of the broadening of the coupled modes around the anticrossing point by 40–60 cm^{-1} compared to values at very large n_e for the higher branch (LOPC+) and at very small n_e for the lower branch (LOPC−). They utilized the classical dielectric function consisting of the sum of a term of polar-optical phonon and a free-carrier Drude-type one. Although we utilized explicit expression of the LOPC modes of Eq. (1), the physical meaning of the obtained broadening factors at 300 K is thought to be the same: the enhancement of LOPC around anticrossing region. Thus, the enhancement of $\Delta\gamma_j$'s only around the anticrossing region and the larger $\Delta\gamma_+$ than $\Delta\gamma_-$ show the characteristic feature of the strong LOPC.

In Fig. 3(a), there is some scattering of data points in a range of 70–120 cm^{-1} for the LOPC− mode in the n_e/m_e^* region of less than 1×10^{19} cm^{-3}, which corresponds to about 5×10^{17} cm^{-3} of n_e. Figure 5 shows the γ_p values as a function of full width at half maximum (FWHM) of $(10\bar{1}2)$

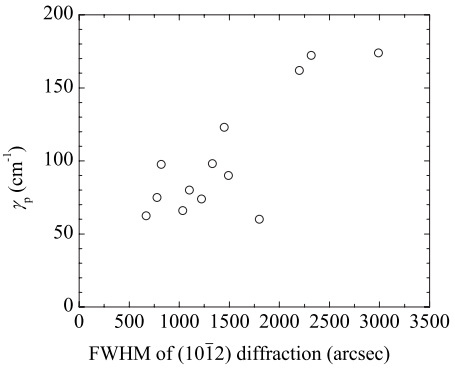

FIG. 5. Relationship between γ_p and the FWHM of (10$\bar{1}$2) diffraction peak in x-ray rocking curve.

diffraction peak. We find that γ_p increases with the increase in FWHM of (10$\bar{1}$2) diffraction peak with some extent of scattering of the data points, but has no correlation with that of (0002) diffraction peak in Table I. This result means that the edge dislocation affects the electron scattering rate. There are issues on the dominant contribution of electron scattering at dislocations in the dependence of Hall mobility on temperature.[14,15] Thus, in the present status of InN crystal quality, the scattering at crystal defects such as dislocations is estimated to contribute to the increase in γ_p in addition to the intrinsic carrier scattering by Fröhlich interaction. It was reported that the edge-type dislocation had a density of 2×10^{10} cm^{-2} for a sample made by our MBE system, which means that dislocations exist every 70 nm. This means that the electron scattering at dislocations cannot be neglected also for our samples. Although at low temperature we stated that LOPC modes are established despite these high-density dislocations, the effect of these scattering on the temperature dependence of the broadening factor is unknown. At present, we have no information of the effect of the temperature increase on the scattering by distorted lattice vibrations at defects.

Recently, Chang *et al.* reported the LOPC modes for the A_1 mode and the damping time of 60–120 fs, which corresponds to 270–560 cm^{-1} as mode energy broadening, for n_e of 2×10^{18} cm^{-3}. This broadening is larger than our result of about 100 cm^{-1} for the E_1 mode. For other reports, there are no clear evidences of the establishment of LOPC for the A_1 mode. Although the mechanism of charge-density fluctuation in crystal was proposed, the mechanism on the anisotropy in the scattering process is not uncovered.

The increase in $\varepsilon(\infty)/\varepsilon_0$ with the increase in n_e/m_e^* indicates the degradation of crystal quality of these samples with the increase in crystal defects. However, the broadening factors of small γ_-, $\Delta\gamma_-$, and $\Delta\gamma_+$ of samples with high n_e/m_e^* agree with the tendency of other samples dominated by the LOPC scheme. Thus, the electron-phonon interaction behavior is preserved even for our samples with high residual electron density, though the crystal quality affects $\varepsilon(\infty)/\varepsilon_0$.

V. CONCLUSION

IR reflectance spectra of InN samples were investigated for an n_e/m_e^* range of $4\times10^{18}-1\times10^{20}$ cm^{-3}. The broadening factors of the plasmon and higher- and lower-energy branches of LOPC of the E_1(LO) mode for these typical InN samples showed the clear behavior of the coupled system, despite the high dislocation density of order of 10^9 or 10^{10} cm^{-2}. It was shown that the increase of these broadening factors with the temperature increase was enhanced in the level anticrossing region of LOPC+ and LOPC− modes. This n_e/m_e^* position of about $(3-4.5)\times10^{19}$ cm^{-3} agrees with the theoretical estimation. These increases in the broadening factors are also evidence of the establishment of strong LO phonon-plasmon coupling for the E_1(LO) mode. Compared to the recent report on the LOPC for A_1(LO), smaller broadening for E_1(LO) was observed here.

ACKNOWLEDGMENTS

The authors are grateful to Mukai of Nichia Corporation for providing us GaN templates. This study is partially supported by the Ministry of Education, Science, Sports and Culture of Japan, Grant-in-Aid for Science Research on Priority Areas, No. 18069002.

*Email address: ishitani@faculty.chiba-u.jp

[1] J. Wu, W. Walukiewicz, W. Shan, K. M. Yu, J. W. Agar, S. X. Li, E. E. Haller, H. Lu, and W. J. Schaff, J. Appl. Phys. **94**, 4457 (2003).

[2] R. Goldhahn, A. T. Winzer, V. Cimalla, O. Ambacher, C. Cobet, W. Richter, N. Esser, J. Furthmüller, F. Bechstedt, H. Lu, and W. J. Schaff, Superlattices Microstruct. **36**, 591 (2004).

[3] Y. Ishitani, K. Xu, W. Terashima, H. Masuyama, M. Yoshitani, N. Hashimoto, S. B. Che, and A. Yoshikawa, *GaN and Related Alloys—2003*, MRS Symposia Proceedings No. 798 (Materials Research Society, Pittsburgh, 2004), p. 207.

[4] T. V. Shubina, S. V. Ivanov, V. N. Jmerik, D. D. Solnyshkov, V. A. Vekshin, P. S. Kop'ev, A. Vasson, J. Leymarie, A. Kavokin, H. Amano, K. Shimono, A. Kasic, and B. Monemar, Phys. Rev. Lett. **92**, 117407 (2004).

[5] A. Kasic, M. Schubert, Y. Saito, Y. Nanishi, and G. Wagner, Phys. Rev. B **65**, 115206 (2002).

[6] J. Wu, W. Walukiewicz, W. Shan, K. M. Yu, J. W. Ager III, E. E. Haller, H. Lu, and W. J. Schaff, Phys. Rev. B **66**, 201403(R) (2002).

[7] S. P. Fu and Y. F. Chen, Appl. Phys. Lett. **85**, 1523 (2004).

[8] B. R. Nag, Phys. Status Solidi B **237**, R1 (2003).

[9] Y. Ishitani, W. Terashima, S. B. Che, and A. Yoshikawa, Phys. Status Solidi C **3**, 1850 (2006).

[10] B. B. Varga, Phys. Rev. **137**, A1896 (1965).

[11] M. Giehler and E. Jahne, Phys. Status Solidi B **73**, 503 (1976).

[12] K. S. Singwi and M. P. Tosi, Phys. Rev. **147**, 658 (1966).

[13] M. Ramsteiner, O. Brandt, and K. H. Ploog, Phys. Rev. B **58**,

1118 (1998).
[14] X. Wang and A. Yoshikawa, Prog. Cryst. Growth Charact. Mater. **48-49**, 42 (2004).
[15] X. Wang, S.-B. Che, Y. Ishitani, and A. Yoshikawa, Appl. Phys. Lett. **90**, 151901 (2007).
[16] J. S. Thakur, R. Naik, V. N. Naik, D. Haddad, G. W. Auner, H. Lu, and W. J. Schaff, J. Appl. Phys. **99**, 023504 (2006).
[17] K. A. Wang, Y. Cao, J. Simon, J. Zang, A. Mintairov, J. Merz, D. Hall, T. Kosel, and W. S. Jena, Appl. Phys. Lett. **89**, 162110 (2006).
[18] V. Yu. Davudov, V. V. Emtsev, I. N. Goncharuk, A. N. Smirnov, V. D. Petrikov, V. V. Mamutin, V. A. Vekshin, S. V. Ivanov, M. B. Smirnov, and T. Inushima, Appl. Phys. Lett. **75**, 3297 (1999).
[19] V. Darakchieva, P. P. Paskov, E. Valcheva, T. Pascova, M. Schubert, C. Bundesmann, H. Lu, A. J. Schaff, and B. Monemar, Superlattices Microstruct. **36**, 573 (2004).
[20] T. Inushima, T. Shiraishi, and V. Y. Davydov, Solid State Commun. **110**, 491 (1999).
[21] Y.-M. Chang, C. T. Chuang, C. T. Chia, K. T. Tsen, H. Lu, and W. J. Schaff, Appl. Phys. Lett. **85**, 5224 (2004).
[22] T. Inushima, M. Higashiwaki, and T. Mutsui, Phys. Rev. B **68**, 235204 (2003).
[23] F. Demangeot, C. Pinquier, J. Frandon, M. Gaio, O. Briot, B. Maleyre, S. Ruffenach, and B. Gil, Phys. Rev. B **71**, 104305 (2005).
[24] J. W. Pomeroy, J. W. M. Kubal, H. Lu, W. Schaff, X. Wang, and A. Yoshikawa, Appl. Phys. Lett. **86**, 223501 (2005).
[25] A. S. Barker, Jr., Phys. Rev. **132**, 1474 (1963).
[26] M. Schubert, T. E. Tiwald, and C. M. Herzinger, Phys. Rev. B **61**, 8187 (2000).
[27] E. O. Kane, J. Phys. Chem. Solids **1**, 249 (1957).
[28] I. Mahboob, T. D. Veal, C. F. McConville, H. Lu, and W. J. Schaff, Phys. Rev. Lett. **92**, 036804 (2004).
[29] L. F. J. Piper, T. D. Veal, C. F. McConville, H. Lu, and J. Schaff, Appl. Phys. Lett. **88**, 252109 (2006).
[30] R. T. Holm and E. D. Palik, J. Vac. Sci. Technol. **13**, 889 (1976).
[31] Y.-M. Chang, H. W. Chu, C.-H. Schen, H.-Y. Chen, and S. Gwo, Appl. Phys. Lett. **90**, 072111 (2007).